Title

HydE Catalytic Mechanism Is Powered by a Radical Relay with Redox-Active Fe(I)-Containing Intermediates.

Journal

Journal of the American Chemical Society, 147(6)

Authors

Chen, Nanhao

Rao, Guodong

Tao, Lizhi

et al.

Publication Date

2025-02-12

DOI

10.1021/jacs.4c12668

Peer reviewed

JACS
JOURNAL OF THE AMERICAN CHEMICAL SOCIETY

pubs.acs.org/JACS
Article

HydE Catalytic Mechanism Is Powered by a Radical Relay with Redox-Active Fe(I)-Containing Intermediates

Nanhao Chen, Guodong Rao, Lizhi Tao, R. David Britt,* and Lee-Ping Wang*

Cite This: J. Am. Chem. Soc. 2025, 147, 4800−4809
Read Online

ACCESS | Metrics & More | Article Recommendations | Supporting Information

ABSTRACT: [FeFe]-hydrogenases are enzymes that catalyze the redox interconversion of H^+ and H_2 using a six-iron active site, known as the H-cluster, which consists of a structurally unique $[2Fe]_H$ subcluster linked to a $[4Fe{-}4S]_H$ subcluster. A set of enzymes, HydG, HydE, and HydF, are responsible for the biosynthesis of the $[2Fe]_H$ subcluster. Among them, it is well established that HydG cleaves tyrosine into CO and CN^- and forms a mononuclear $[Fe(II)(Cys)(CO)_2(CN)]$ complex. Recent work using EPR spectroscopy and X-ray crystallography show that HydE uses this organometallic Fe complex as its native substrate. The low spin Fe(II) center is reduced into an adenosylated Fe(I) species, which is proposed to form an Fe(I)Fe(I) dimer within HydE. The highly unusual transformation catalyzed by HydE draws interest in both biochemistry and organometallic chemistry. Due to the instability of the substrate, the intermediates, and the proposed product, experimental characterization of the detailed HydE mechanism and its final product is challenging. Herein, the catalytic mechanism of HydE is studied using hybrid quantum mechanics/molecular mechanics (QM/MM) molecular dynamics simulations. A radical relay mechanism was found for the cleavage of the cysteine S−Cβ bond that is energetically favored with respect to a closed-shell mechanism involving unconventional proton transfer. In addition, we propose a pathway for the dimerization of two Fe(I) complexes within the HydE hydrophobic cavity, which is consistent with the recent experimental result that HydF can perform [FeFe]-hydrogenase maturation with a synthetic dimer complex as the substrate. These simulation results take us further down the path to a more complete understanding of these enzymes that synthesize one of Nature's most efficient energy conversion catalysts.

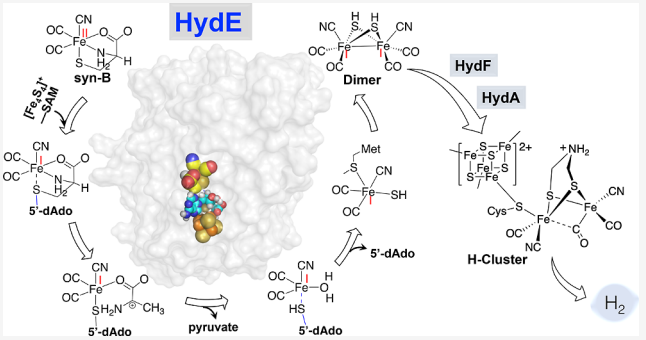

1. INTRODUCTION

Hydrogenase enzymes occur in [FeFe], [NiFe], and [Fe]-only forms and catalyze microbial H_2 uptake, with the first two forms serving as reversible redox catalysts of the reaction $[H_2 \leftrightarrow 2H^+ + 2e^-]$.[1−3] The hydrogenases provide cellular energy and leveling of redox potential, enabling crucial metabolic pathways. In addition, there is much interest in using them in forming H_2 as a fuel, for example, from protons and electrons produced by solar water splitting.[4]

Much of our efforts have been focused on the assembly of the catalytic "H-cluster" of the [FeFe]-hydrogenases,[5−13] which consists of a $[4Fe{-}4S]_H$ subcluster linked to an organometallic $[2Fe]_H$ subcluster (Figure 1, left, "HydA").[14,15] The $[2Fe]_H$ subcluster is synthesized and linked with the [4Fe−4S] cluster by three Fe−S "maturase" enzymes—HydE, HydF, and HydG, in a complex process that involves inorganic, organometallic, and organic radical chemistry.[5,16−20]

The H-cluster assembly starts with HydG, which is a member of the radical *S*-adenosyl-*L*-methionine (SAM) family of enzymes that employ a [4Fe−4S] cluster to catalyze the reductive cleavage of SAM, generating a 5′-deoxyadenosyl radical (5′-dAdo•).[21−24] 5′-dAdo• then abstracts an H atom from the given enzyme's substrate, tyrosine. In HydG, there is a single auxiliary Fe−S cluster found in a unique five-Fe motif[10] (Figure 1, top left). Our previous research has pointed to HydG's prominent role in $[2Fe]_H$ subcluster biosynthesis by converting tyrosine, cysteine, and Fe(II) from the fifth "dangler" Fe site of this auxiliary cluster into an organometallic $[Fe(II)(Cys)(CO)_2(CN)]$ "synthon"[11] that then undergoes dimerization and other transformations catalyzed by HydE and HydF to produce the $[2Fe]_H$ subcluster. A detailed step-by-step mechanism of HydG was determined using computational studies that employed a hybrid quantum mechanical/molecular mechanical (QM/MM) model.[25] The tyrosine substrate is converted to CO and CN and transferred to the auxiliary cluster

Received: September 12, 2024
Revised: January 17, 2025
Accepted: January 17, 2025
Published: January 30, 2025

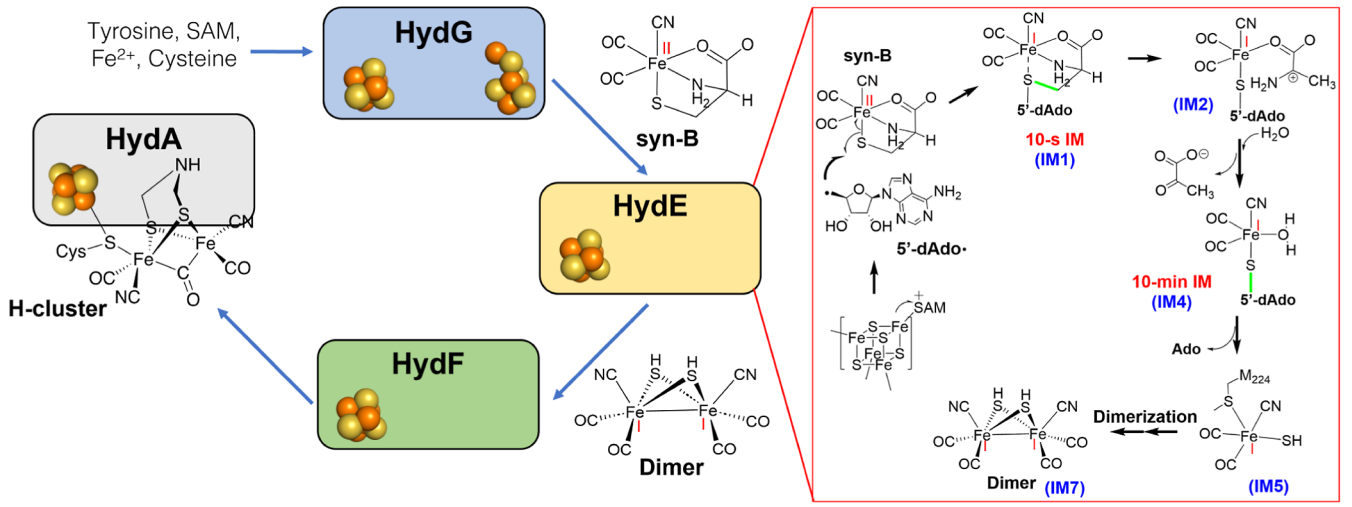

Figure 1. Proposed reaction scheme of HydE catalysis in the published literature. Left: The Fe−S clusters of HydG, HydE, and HydF and the $[4Fe\text{-}4S]_H$ subcluster of [FeFe]-hydrogenase (HydA) are shown using spheres (Fe, orange, and S, yellow). The proposed products of HydG and HydE and the $[2Fe]_H$ subcluster of HydA are shown as line drawings. Right: Overview of the catalytic mechanism of HydE, including the three experimentally detected "10 s intermediate" (IM1), "10 min intermediate" (IM4), penta-coordinate-proposed protein-bound intermediate (IM5), and proposed dimer product (IM7). The blue labels are used for important structures in the current study.

where they coordinate to the "dangler" Fe to yield the experimentally observed $[Fe(II)(Cys)(CO)_2(CN)]$ complex.

The use of a synthetic $[Fe(II)(Cys)(CO)_2(CN)]$ replica of this proposed HydG product, "Syn-B", showed that HydG itself can then be eliminated in the synthesis of an active H-cluster (Figure 1).[26] More recently, Omeiri et al. showed using X-ray crystallography that HydG is capable of transferring the synthon directly to HydE.[27] EXAFS studies that compared the H-cluster structure when selenocysteine was substituted for cysteine in Syn-B showed that the bridging S/Se of the binuclear cluster is sourced from this cysteine S/Se. Also, HYSCORE (hyperfine sublevel correlation spectroscopy) reveals no $^{13}C/^{15}N$ coupling using $^{13}C3,^{15}N$-cysteine in the maturation, although $^{13}C3$ pyruvate accumulates in the maturation media, demonstrating that the S−Cβ bond of cysteine must be cleaved in the maturation reaction. Berggren et al. reported that the existence of the azadithiolate (ADT) bridging ligand is essential for the maturation of the [FeFe]-hydrogenase,[28] and we showed that the CH_2NHCH_2 fragment of the ADT bridging ligand is actually sourced from serine and ammonium.[29−31] In addition, a chemical mimic of the [2Fe] subcluster can completely activate the [FeFe]-hydrogenase without HydE, HydF, and HydG.[32]

We showed that this S−Cβ bond cleavage of cysteine is catalyzed by the second radical SAM maturase, HydE.[33] The radical SAM-generated 5′-dAdo$^\bullet$ attacks the cysteine sulfur to form a cross-linked Fe(I) adenosyl complex, giving an $S = \frac{1}{2}$ EPR signal that peaks at about 10 s in the reaction. The S−Cβ bond cleavage follows the formation of this species, resulting in a different Fe(I) EPR signal arising from a different complex, which we now think is a penta-coordinate $[Fe(I)S(CO)_2(CN)]$ species.[34−36] This new EPR signal peaks at about 10 min and then decays. We discussed this in light of the tendency for such penta-coordinate Fe(I) organometallic species to dimerize, which would give rise to an antiferromagnetically coupled, EPR silent reaction product $[Fe_2S_2(CO)_4(CN)_2]$. In 2021, Rohac et al. published a crystal structure showing the binding conformation of Syn-B within HydE.[34] By triggering the radical chemistry of HydE using a chemical reducing agent prior to crystallization, it was found that HydE converts Syn-B into a new pentacoordinate $[Fe(I)S(CO)_2(CN)]$ intermediate coordinated to the methionine M224. This intermediate is further hypothesized to undergo dimerization in HydE, in which residue M291 transiently binds one Fe(I) complex while a second complex is produced. Recently, Zhang et al. showed that the complex $[Fe_2(\mu\text{-}SH)_2(CN)_2(CO)_4]^{2-}$, a synthetic analogue of this proposed HydE product, allows the maturation of HydA with only HydF,[37] which is consistent with the hypothesis that the dimer is the product of HydE.

The experimental results support a mechanism of HydE shown on the right of Figure 1. In this mechanism, HydE catalyzes radical addition of 5′-dAdo$^\bullet$ on the cysteine sulfur of the $[Fe(II)(Cys)(CO)_2(CN)]$ complex, the HydG product, forming the "10 s intermediate". The cysteine ligand undergoes S−Cβ bond cleavage, and further substitutions then dissociate from the complex as pyruvate, forming the "10 min intermediate". 5′-dAdo is cleaved off, and Fe(I) associates with the M224 side chain resulting in the penta-coordinate $[Fe(I)(M224)S(CO)_2(CN)]$-proposed protein-bound intermediate.[34] Two equivalents of $[Fe(I)S(CO)_2(CN)]$ then undergo dimerization within HydE to afford $[Fe_2S_2(CO)_4(CN)_2]$, which is the hypothesized product of HydE. This proposed mechanism raises several key questions, such as

1. How does the radical SAM chemistry of HydE interacting with its $[Fe(II)(Cys)(CO)_2(CN)]$ substrate lead to the cleavage of the S−Cβ bond of the cysteine ligand?
2. Subsequently, the S−C5(Ado) bond formed in the initial radical step must be cleaved in the formation of the Fe_2S_2 diamond core in the product. How does this reaction proceed?
3. Is it feasible that the Fe_2S_2 diamond core forms within HydE itself, as opposed to externally? If so, what detailed mechanism may be used to form this dimer, and how is it then released to transfer to HydF to complete the ADT bridging ligand?

Here, we report the results of a computational QM/MM study on the mechanism of HydE to address the mechanistic questions. Our main findings are that the S−Cβ cleavage of Cys

https://doi.org/10.1021/jacs.4c12668
J. Am. Chem. Soc. 2025, 147, 4800−4809

proceeds in a radical relay mechanism with the substrate Fe participating in a redox-active way, briefly transferring an electron to Cys Cβ to effect a homolytic bond cleavage and resulting in an Fe(II) intermediate with a Cβ-radical in the first coordination sphere; this radical is transferred back to Fe(I) in a relay that involves the K309 lysine residue of HydE. An analogous radical relay mechanism is invoked for the radical cleavage of the S−C5(Ado) bond in the "10 min intermediate", releasing the 5′-dAdo$^\bullet$ radical and producing the Syn-B that is capable of coordinating to M224. Finally, two such Fe(I) complexes coordinated to M224 and M291 undergo dimerization to yield the $[Fe_2S_2(CO)_4(CN)_2]$ product. Overall, the computational mechanism shows how HydE is able to carry out the conversion of $[Fe(II)(Cys)(CO)_2(CN)]$ into the dimer product using radical chemistry that involves highly interesting redox noninnocence of first coordination sphere ligands as key steps. Further, this mechanism is consistent with all published experimental observations of HydE and shows that dimerization is thermodynamically and kinetically accessible within the enzyme, providing further evidence that HydF is not needed to carry out this crucial step in the synthesis of the organometallic $[2Fe]_H$ subcluster of the hydrogenase-active site.

2. METHODS

The calculations in this study mainly consist of free energy profiles of elementary reaction steps that are computed using molecular dynamics (MD) simulations of a hybrid quantum mechanical/molecular mechanical (QM/MM) model of HydE. To construct the model, a structure of a HydE mutant (PDB ID: 7O1O) from Rohac et al.[34] with bound Syn-B and *S*-adenosyl-*L*-homocysteine (SAH) ligands was chosen as the base structure for modeling as it closely matched our system of interest. The mutation is missing an $[Fe_2S_2]$ cluster in the C-terminal region of HydE but is not expected to affect the catalysis. The inactive SAH was substituted by the active SAM, which is the exact substrate in HydE. The protonation states of all residues were decided according to their standard side chain pK_a values and the experimental pH value (7.0). In several of the simulations, the lysine residue K309 was deprotonated to study its possible role as a proton acceptor.

The classical portion of the QM/MM model used the AMBER-FB15 force field for the protein,[38] which includes parameters for deprotonated lysine, and the TIP3P-FB model for water.[39] The GAFF small molecule force field was used to parameterize the nonmetallic ligands including SAM, cysteine, CO, and CN^-;[40] the HydE $[Fe_4S_4]$ cluster was modeled using force field parameters from ref 41 for iron−sulfur clusters, and the Fe(II) ion of Syn-B was modeled using force field parameters from ref 42. The structure preparations were all done with the help of *tleap* in Amber16.[43]

Prior to running any QM/MM simulations, a sequence of classical MD simulations were carried out to relax any close contacts and other defects caused by modeling in the initial structure. In these classical simulations, the coordination environment of Fe(II) was restrained by adding harmonic potential terms on the distances and angles between the diatomic ligands and Fe(II) with the force constants equal to 50 kcal/mol/Å^2 and 100 kcal/mol/rad^2, respectively. First, five thousand steps of energy minimization were carried out with the protein heavy atoms restrained to the experimental positions (the restraint constant is 20 kcal/mol/Å^2), followed by another five thousand steps of minimization with the protein restraints removed. Next, a 200 ps MD simulation under NVT conditions, followed by a 200 ps simulation under NPT conditions, was carried out in order to heat the system to 300 K and equilibrate the density under 1 atm pressure. Finally, a 50 ns MD simulation under NVT conditions was carried out. Each of these simulation steps used the final structure from the preceding step, and the final structure of the 50 ns simulation was used as the starting point in the QM/MM simulations. The time step of all MD simulations was set to 1 fs, a Langevin thermostat algorithm with a collision frequency of 1.0 ps^{-1} was set to control the temperature, and a Berendsen barostat was used to control the pressure in the NPT run. The cutoff values for both short-range electrostatics and van der Waals interactions were set to 12 Å, while the particle-mesh Ewald method was chosen to describe the long-range summation of the electrostatic interactions.

The QM/MM simulations were carried out using the Qchem 4.0[44]/AMBER12[43] software packages for the QM and MM regions, respectively, and joined together using a pseudobond Q-Chem/AMBER interface.[45] These simulations employ an electrostatic embedding model in which the MM partial charges have electrostatic interactions with the nuclear charges and electron density in the QM region. Different QM regions were used during the catalytic process depending on which region of the protein was involved in the reactivity for each elementary step. Based on the other QM/MM simulations on iron−sulfur proteins,[46] the QM regions were described by the unrestricted B3LYP density functional approximation, and the basis set used was def2-SVP for most atoms and def2-SV(P) for Fe. The chosen level of theory was validated by rerunning selected calculations using a modified BP86 functional consisting of 5% HF exchange and 95% B88 exchange and the larger def2-TZVP basis set (Figures S18−S24); these results showed a difference of <4 kcal/mol in the activation barriers from our chosen level of theory, which were overall consistent with ref 25. In instances where the QM and MM regions are covalently bonded, we adopted a pseudobond approach in which the boundary atom on the MM side of the covalent bond is modeled using seven electrons, a spherically symmetric pseudopotential and an STO-2G basis set.[47] The QM atoms directly bonded to the boundary atom used the 6-31G* basis set.

The catalytic reactions were studied by the following procedure. The initial structure was obtained by the energy minimization of the entire QM/MM system. A reaction coordinate (RC) driving procedure is then performed, which comprises a series of energy minimizations in which the chosen RC, defined by using linear combinations of one or more interatomic distances, was constrained to values ranging from the reactant to the product. Following this, QM/MM MD simulations in the *NVT* ensemble with umbrella sampling along the defined RC were carried out using the same time step and thermostat as in the classical MD simulations, totaling about 15 ps for each window. The energies and structures for the last 10 ps of simulation data were retained for structural analysis and generating the free energy profile with the weighted histogram analysis method.[48,49] Approximate transition-state structures shown in this paper are representative structures taken from simulations at the highest point on the corresponding free energy profile.

3. RESULTS AND DISCUSSION

3.1. Formation of the "10 s Intermediate". The catalytic cycle of HydE, a radical SAM enzyme, is initialized by the decomposition of SAM and the generation of 5′-dAdo$^\bullet$, which triggers downstream radical reactions. Since the SAM decomposition is a well-known and well-studied biochemical reaction in both experiments and computations, herein, we only use RC driving without further free energy simulations (Figure S1) to compute the reaction pathway resulting in 5′-dAdo$^\bullet$. Following this, we studied the radical addition of SAM to cysteinyl sulfur, one of the key reactions in the HydE catalytic process (Figures 2 and S2). Although SAM enzymes generally follow a reactivity pattern of using the 5′-dAdo$^\bullet$ to abstract an H atom from the substrate, HydE instead uses 5′-dAdo$^\bullet$ to carry out radical addition. According to the free energy profile in Figure 2A, this C−S radical addition is thermodynamically feasible with an activation free energy ($\Delta G^\ddagger$) and reaction free energy (ΔG) of 5.1 and −11.1 kcal/mol, respectively, abbreviated here as ($\Delta G^\ddagger$, ΔG) = (5.1, −11.1) kcal/mol. As shown in Figure 2, the spin density in 5′-dAdo$^\bullet$ is directed toward the sulfur atom of Syn-B, providing a good orientation for the C−S addition (Figure 2B); a representative transition-state structure is shown in Figure S2. During the addition

https://doi.org/10.1021/jacs.4c12668
J. Am. Chem. Soc. 2025, 147, 4800−4809

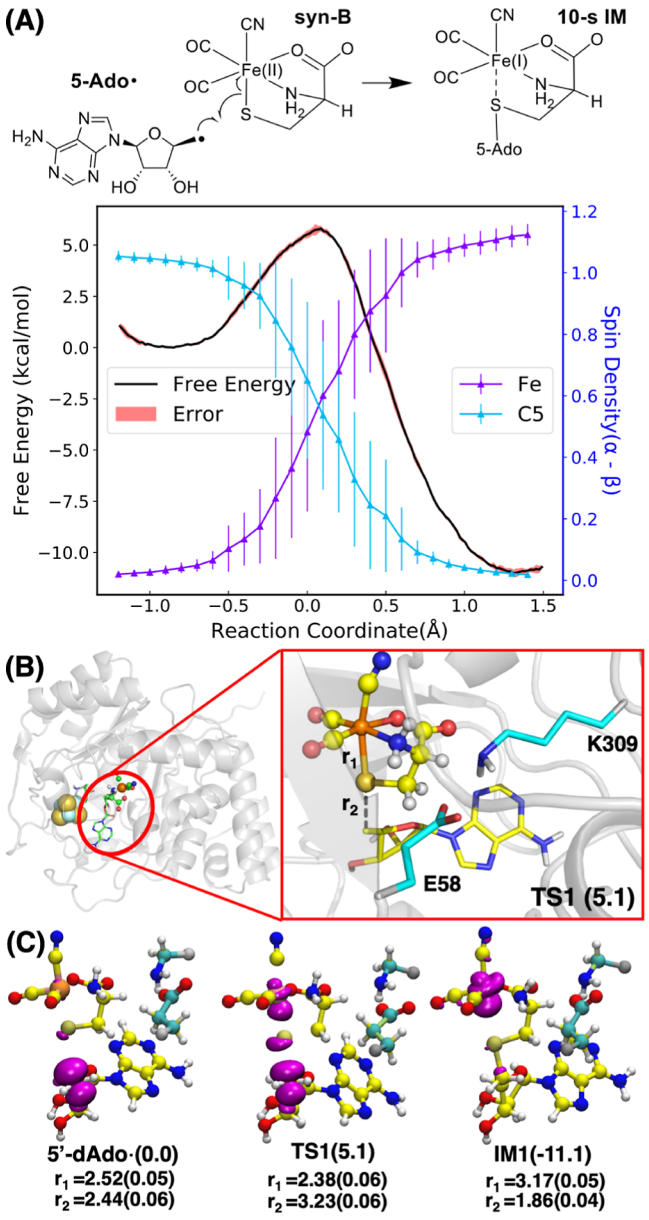

Figure 2. Formation of the "10 s intermediate" by radical addition of 5′-dAdo• to the cysteinyl sulfur of Syn-B. The free energy profile of the reaction is displayed in the top panel (A) with the spin density changes of 5′-dAdo• C5 and Syn-B Fe. Here, the RC is defined as $r_1 - r_2$, where r_1 and r_2 represent the distances of Fe−S and S−C5, respectively. The transition-state structure of this addition reaction is shown in ball and stick representation in the middle panel (B) highlighting the key distances along the reaction. The spin densities of key states are drawn in the bottom panel (C) to show the radical transfer during the reaction. The spin density isosurfaces are colored in magenta. Energies and key distances are given in kcal/mol and Å, respectively.

process, the spin density was observed to transfer from C5 in 5′-dAdo• to Fe(II) as shown in Figure 2C, corresponding to a formal reduction to Fe(I). This Fe(I) structure labeled IM1 in Figure 2C has been previously detected in EPR experiments and named the "10 s intermediate".[33] We observed that the C−S addition causes the S to dissociate almost completely from Fe(I) as the latter distance increased from 2.4 to 3.2 Å. The resulting ligand is termed an *S*-adenosyl cysteine (SAC) molecule, equivalent to a demethylated SAM.

3.2. Conversion of the "10 s Intermediate". *3.2.1. Cysteine Decomposition Pathway via the Radical Relay Mechanism.* Experiments show that the "10 s intermediate", i.e., IM1 formed in the previous step, is converted to another intermediate on a 10 min time scale that occurs concurrently with the release of pyruvate. The cleavage of the S−Cβ bond of the cysteine ligand is a key step in this conversion and was initially proposed as a β-elimination involving a proton transfer from the Hα of cysteine to a basic residue, followed by S−Cβ bond cleavage leading to a 5′-*S*-dAdo species and dehydroalanine (dHA) coordinated to Fe(I).[33] In this study, we found that the β-elimination mechanism is kinetically prohibitive, and a radical mechanism was found to be a feasible alternative as described below.

The possible candidates for the proton acceptor in the β-elimination include the side chains of glutamate E58 and lysine K309, which form a salt bridge in the crystal structure.[34] The proton transfer from Cα to the K309 side chain and the heterolytic S−Cβ bond dissociation were found to occur in a concerted fashion with an activation free energy of $\Delta G^{\ddagger} \sim 40$ kcal/mol relative to IM1 (Figures S3 and S4). This step produces a metastable structure-labeled PIM1.1 (ΔG = +22.3 kcal/mol, here the letter "P" refers to the Hα proton-transfer pathway) that can convert into another structure labeled PIM1.2 via ligand exchange, in which 5′-*S*-dAdo coordinates to Fe(I), while the dHA amine group dissociates. The alkene carbon of dHA is protonated by K309, while the amine is deprotonated by E58, converting it into a 2-iminopropanoate ligand (PIM2, Figure S5). The rate constant corresponding to $\Delta G^{\ddagger} \sim 40$ kcal/mol can be estimated from the Eyring equation as $\sim 10^{-17}$ s^{-1} at T = 300 K and is kinetically prohibitive.[50]

We computationally searched for alternatives to the β-elimination pathway and found a radical relay mechanism for S−Cβ bond cleavage with a much lower free energy barrier (Figure 3). In this mechanism, the first step is the homogeneous cleavage of S−Cβ and oxidation of Fe(I) to Fe(II), which can also be viewed as S atom abstraction from cysteine by Fe(I). This step reforms the Fe−S coordination bond and leaves a primary radical at Cβ, labeled IM1.1. Next, the K309 side chain transfers one hydrogen to Cβ (IM1.2) and then abstracts the Hα from Cα, converting the primary radical to a more stable secondary radical (IM1.3). The radical transfers back to Fe(II) via an Fe−N coordination bond cleavage, reducing it to Fe(I) again (IM2).

Three of the free energy barriers of the reaction are within the range of $\Delta G^{\ddagger}$ = 26−28 kcal/mol, with respect to IM1. Although there is no measured experimental rate constant, we estimate it to be $k \sim 10^{-3}$ s^{-1} based on the 10 min time scale of the reaction; this may be converted to $\Delta G^{\ddagger} \sim 21$ kcal/mol using classical transition-state theory. Therefore, our calculations somewhat overestimate the activation energy, and this is consistent with DFT studies on other radical SAM enzymes where B3LYP is shown to overestimate the barrier by 4−8 kcal/mol.[51] Our calculated free energy barriers are also close to our previous result of $\Delta G^{\ddagger}$ = 26.3 kcal/mol for the Fe−S cluster-induced decomposition of SAM in HydG,[25] a well-known reaction, as well as the SAM decomposition calculation in HydE (Figure S1), indicating that barriers in this range are competitive on biological time scales.

The energy profiles and the key structures with their spin densities are displayed in Figure 3A, and structures of transition states are detailed in Figures S6−S8. This S−Cβ bond homogeneous cleavage is endothermic with ($\Delta G^{\ddagger}$, ΔG) = (26.0, 10.9) kcal/mol, yielding the IM1.1 state. IM1.1 contains

https://doi.org/10.1021/jacs.4c12668
J. Am. Chem. Soc. 2025, 147, 4800−4809

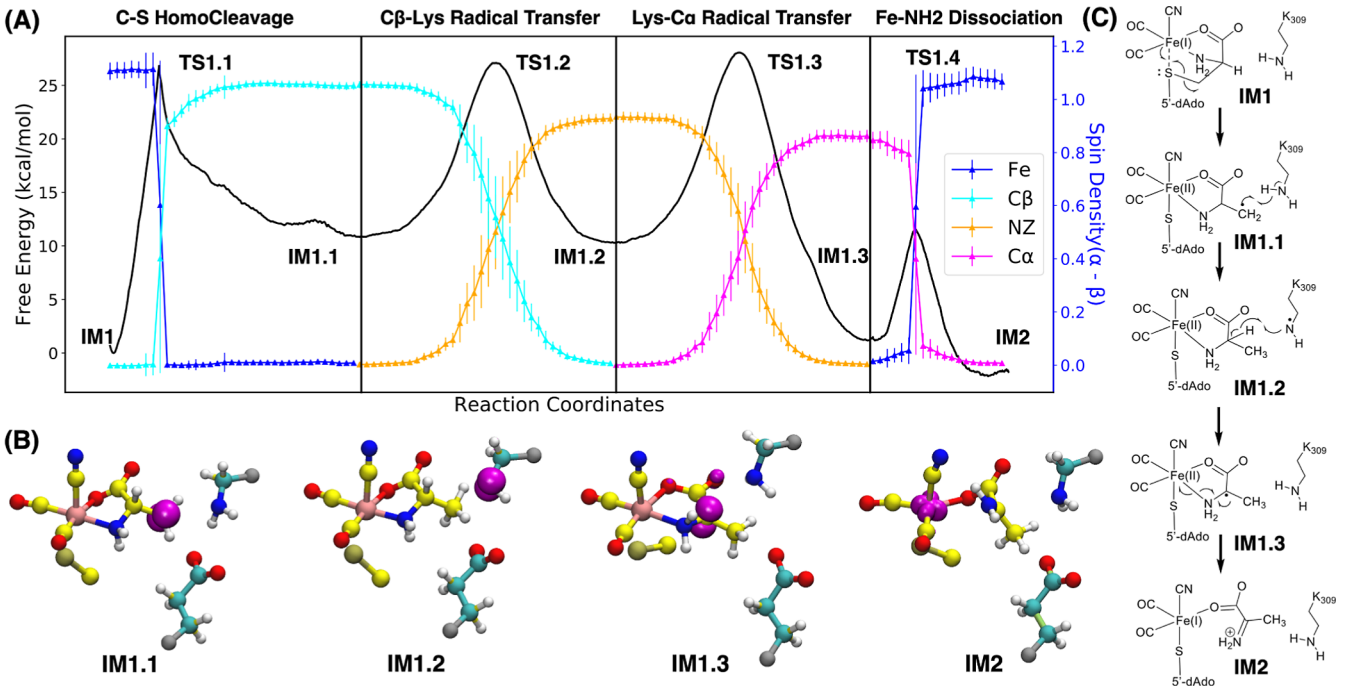

Figure 3. Radical relay mechanism of cysteine decomposition in HydE. (A) Free energy profile (black curve) and the spin densities on key atoms for elementary steps. (B) 3-D structures of intermediates with spin density isosurfaces shown in magenta. (C) Reaction scheme for the radical relay pathway showing the movement of electrons.

an unstable primary radical on Cβ, and it is converted to a secondary radical on Cα (IM1.3) in a two-step mechanism that utilizes the K309 side chain as a temporary radical site. The first H atom transfer from K309 to Cβ (IM 1.1 → IM 1.2) is nearly isoenergetic, with $(\Delta G^{\ddagger}, \Delta G) = (16.3, -0.6)$ kcal/mol, followed by a second H atom transfer from Cα to K309 with $(\Delta G^{\ddagger}, \Delta G) = (17.8, -9.2)$ kcal/mol. The radical character of the states is confirmed by the spin density plots in Figure 3B. We also estimated the free energy barriers of two alternative radical-transfer pathways: the direct H atom transfer from Cα to Cβ had a calculated $\Delta G^{\ddagger} \sim 38$ kcal/mol, and the substitution of K309 by the tyrosine Y306 was found to have $\Delta G^{\ddagger} \sim 45$ kcal/mol, and were not pursued further (Figure S9). The radical mechanism ends with the homolytic dissociation of the Fe−N bond and reduction of Fe(II) to Fe(I); this yields the IM2 state, which is identical to the end point of the unconventional proton-transfer pathway up to some small conformational differences. As the energy diagram in Figure S10 shows, the radical relay mechanism yields the 2-iminopropanoate cation with an overall activation free energy of $\Delta G^{\ddagger} = 28.1$ kcal/mol, which is much lower than the $\Delta G^{\ddagger} \sim 40$ kcal/mol of the closed shell β-elimination mechanism.

Experimental studies on HydE[33] did not observe any radical species between the "10 s intermediate" (IM1) and "10 min intermediate" (IM4); therefore, there is no experimental observation of IM1.1/1.2/1.3/2, although they are expected to be EPR active. This could partly be explained by the computed free energies of IM1.1 and IM1.2 that are significantly higher than IM1. IM1.3 and IM2 have free energies that are close to those of IM1, but they undergo further spontaneous reactions that lead to the release of pyruvate and form the "10 min intermediate".

3.2.2. Conversion of the 2-Iminopropanoate Cation into Pyruvate. According to the experiments, the cysteine in Syn-B is converted into pyruvate on a 10 min time scale and is released as a side product in the HydE catalytic reaction. Our calculations show that pyruvate generation has low activation free energies and involves hydrolysis of the Cα−N bond and several proton-transfer steps that take advantage of the side chains of E58 and K309 as proton repositories. The energy diagram with several critical structures is depicted in Figure 4. The electrophilic Cα of the 2-iminopropanoate ligand first undergoes nucleophilic attack by a water molecule, while the neutral K309 side chain accepts a proton from the water, leaving a hydroxyl group bonded to Cα. This step is facile, and the intermediate containing 2-amino-2-hydroxypropanoate, labeled IM2.1, is energetically favorable compared to the IM2 state $(\Delta G^{\ddagger}, \Delta G) = (8.2, -1.8)$ kcal/mol. Aided by the hydrogen bonding network between the ligand and protein, the K309 side chain can protonate E58, resulting in IM2.2. Next, the elimination of ammonia occurs starting with protonation of the amine by E58, leading to IM2.3, followed by deprotonation of the hydroxyl by K309 and dissociation of NH_3, which has the highest individual barrier of this sequence with $(\Delta G^{\ddagger}, \Delta G) = (14.2, 8.7)$ kcal/mol. The resulting IM2.4 structure contains a pyruvate ligand, and protonation of the free ammonia by K309 ($(\Delta G^{\ddagger}, \Delta G) = (3.7, -9.3)$ kcal/mol) leads to IM3. The entire reaction is exergonic with respect to IM2 containing the 2-iminopropanoate ligand, which is consistent with the lack of EPR evidence for IM2. The pyruvate has been detected in experiments as a side product of the catalytic reaction. We found that pyruvate may be released by substitution of a water molecule, followed by proton transfer from H_2O to the *S*-5′-dAdo sulfur with an overall $(\Delta G^{\ddagger}, \Delta G) \sim (11, 6)$ kcal/mol as shown in Figures S11−S12, leading to the observed "10 min intermediate" observed in experiments (IM4 in Figure 1).

3.3. Conversion of the "10 min Intermediate". In Rohac et al.,[34] a penta-coordinate $[Fe(I)(CO)_2(CN)(Cl)(M-224)]$ complex was observed in the HydE crystal structure by providing a Syn-B substrate and triggering the radical reaction

https://doi.org/10.1021/jacs.4c12668
J. Am. Chem. Soc. 2025, 147, 4800−4809

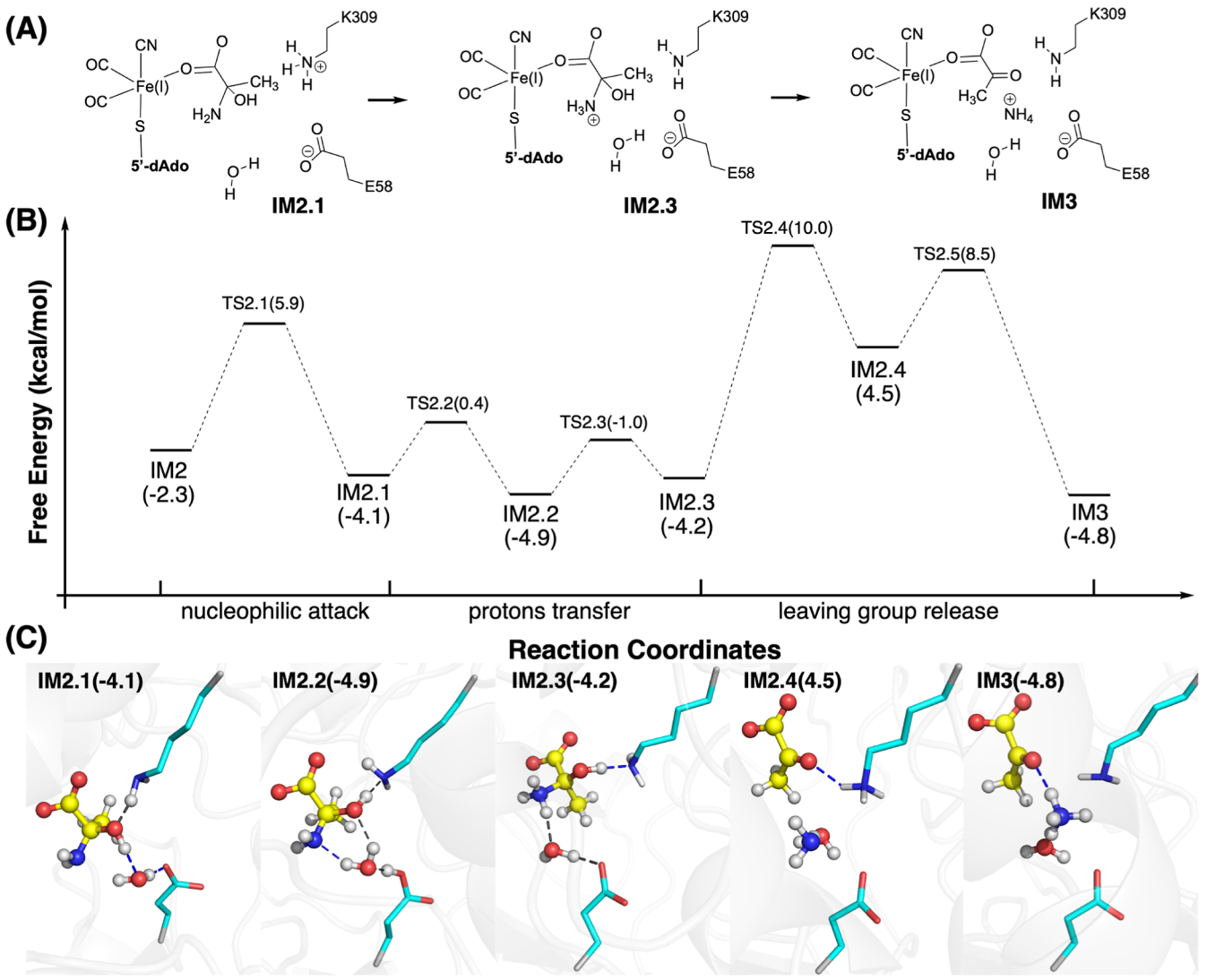

Figure 4. Energy diagram with key structures of the conversion of 2-iminopropanoate into pyruvate, consisting mainly of nucleophilic attack of water (IM2.1), proton transfer (IM 2.2), the protonation of the amine group (IM 2.3), and the release and protonation of ammonia (IM 2.4 and IM3). The top panel (A) depicts the reaction scheme, and the middle panel (B) shows the free energy of the key states in the pyruvate generation process. The bottom panel (C) displays five key stable structures during the pyruvate generation process. The color scheme is identical to the previous figure. Free energies are given in kcal/mol relative to IM1, the "10 s intermediate".

prior to crystallization. Considering the possibility of a diamagnetic Fe_2S_2 dimer product of HydE, the chloride ligand observed in the crystal structure is thought to be substituted by cysteinyl sulfur in the HydE catalytic reaction. Therefore, we searched for a pathway in which *S*-5′-dAdo is cleaved from the "10 min intermediate" (IM4).

A radical relay mechanism for the decomposition of the ″10 min intermediate" was found, shown in Figure 5. This mechanism starts from IM4 and assumes the connecting S atom is protonated, for instance, by deprotonating the water molecule that coordinates to Fe(I) in the previous step, displacing pyruvate via K309/E58 (in Figure S12). In this mechanism, the C5−S bond first undergoes homolytic dissociation, and Fe(I) is temporarily oxidized to Fe(II), resulting in [Fe(II)$(CO)_2$(CN)(SH)(OH)] and a 5′-dAdo$^\bullet$ radical, labeled IM4.1. 5′-dAdo$^\bullet$ then attacks the OH group coordinated to Fe(II), forming a C−OH bond concurrently with the reduction of the Fe center and elongation of the Fe−OH distance, yielding [Fe(I)$(CO)_2$(CN)(SH)] weakly coordinated to an adenosine molecule (IM5 state). The analysis of spin density clearly shows the transfer of unpaired electron density from Fe to the C5′ of 5′-dAdo$^\bullet$, then back to Fe (Figure 5B-C). As shown in Figure 5A, the overall barrier of the conversion reaction of the "10 min intermediate" is $\Delta G^{\ddagger}$ = 28.6 kcal/mol, which is comparable to the conversion of the "10 s intermediate" in which $\Delta G^{\ddagger}$ = 28.1 kcal/mol. The difference in the overall activation free energies is within the margin of error of our density functional but is consistent with the longer half-life of the signal corresponding to the "10 min intermediate".

Thus far, the decomposition of the ″10 min intermediate" has led to IM5, which contains Fe(I) weakly coordinated to adenosine, a good leaving group. The computed pathway is kinetically feasible, but adenosine was not observed above background levels in the experimental HPLC analysis. This may occur if 5′-dAdo$^\bullet$ in IM4.1 abstracts an H atom from the HEPES buffer used in the experiment yielding 5′-dAdo and a secondary HEPES radical,[52] followed by the attack of the latter on the OH ligand of Fe(II) in IM4.1, reducing it to Fe(I) and completing

https://doi.org/10.1021/jacs.4c12668
J. Am. Chem. Soc. 2025, 147, 4800−4809

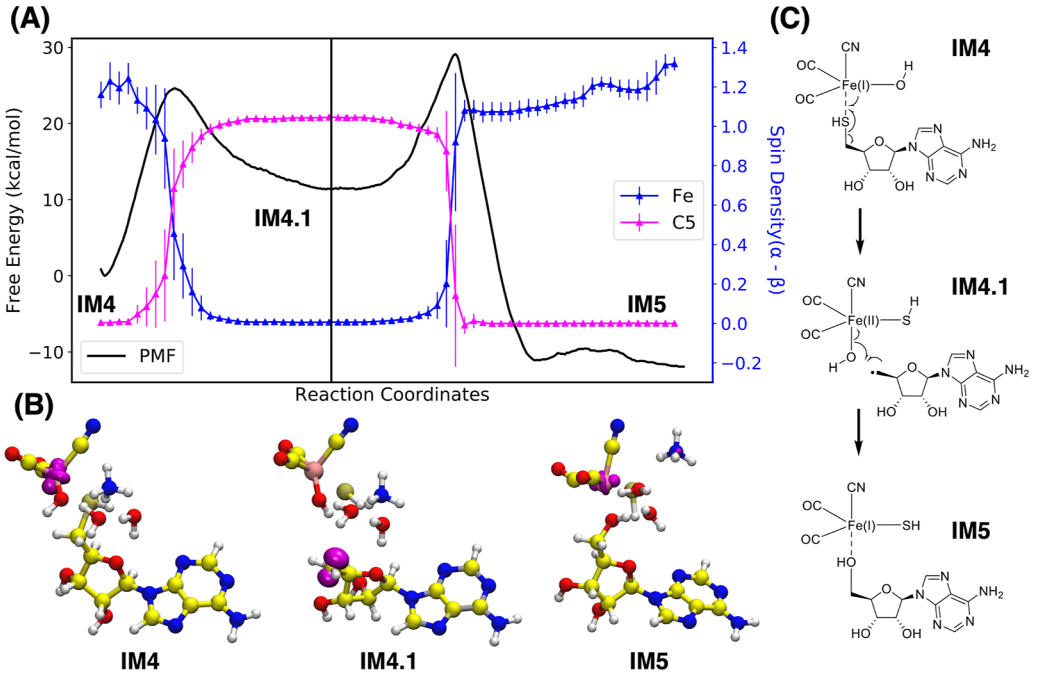

Figure 5. Decomposition mechanism of *S*-5′-dAdo in the "10 min intermediate". Starting with IM4, homolytic cleavage of the C−S bond occurs concomitantly with the oxidation of Fe(I) to Fe(II) and results in a 5′-dAdo• radical. The transfer of OH• from the Fe(II) complex quenches the radical and generates a $[Fe(I)(CO)_2(CN)]$ species weakly coordinated to an adenosine molecule (IM5). (A) Free energy profile (black curve) and the spin densities on key atoms for elementary steps. (B) 3-D structures of intermediates with spin density isosurfaces shown in magenta. (C) Reaction scheme for the radical relay pathway showing the movement of electrons.

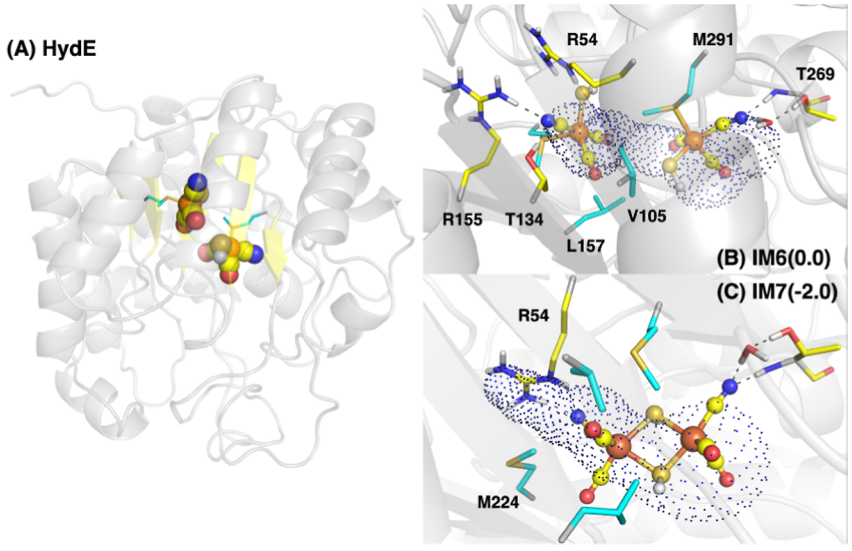

Figure 6. Dimerization mechanism of two $[Fe(I)(CO)_2(CN)(SH)]$ complexes resulting in $[Fe(I)_2(SH)_2(CO)_4(CN)_2]$. (A) Position of the two Fe(I) monomers within the HydE β-barrel. (B) Detail of the structure prior to dimerization with two Fe(I) complexes bound to M291 and M224. The blue dots indicate the approximate boundaries of the hydrophobic cavity of HydE. (C) Product structure of the dimerization reaction. The cavities were determined by the Caver software.[53]

the transfer (Figure S13). Because HEPES is not present in the biological system, we think the biological reaction could either produce adenosine or 5′-dAdo• may perform H atom abstraction from a metabolite that plays a similar role as HEPES.

The experimental structure has Fe(I) coordinated to the M224 side chain, suggesting that it displaces adenosine, but it is more than 8 Å from the generated Fe(I) cluster in our calculations. On the other hand, the M291 residue is much closer to the Fe-cluster in our structure of IM5 as shown in Figure 5. We hypothesize that M291 acts as the first residue to harbor the Fe-cluster, followed by the transfer of the cluster to M224. The replacement of adenosine by M291 was calculated and is shown in Figure S14, and it is found to be energetically very feasible with $(\Delta G^{\ddagger}, \Delta G)$ = (2.5, −0.8) kcal/mol. This step shortens the distance between M224 and Fe(I) to 6 Å, facilitating its transfer to M224 (with $(\Delta G^{\ddagger}, \Delta G)$ = (4.9, −2.4) kcal/mol shown in Figure S15).

3.4. Dimerization Mechanism of Fe(I) Complexes within HydE. A short cavity exists in the HydE structure between M291 and M224, providing enough space for the

https://doi.org/10.1021/jacs.4c12668
J. Am. Chem. Soc. 2025, 147, 4800−4809

$[Fe(I)(CO)_2(CN)(SH)]$ species to be transferred from M291 to M224 and accommodating two Fe(I) clusters simultaneously. This indicates that HydE may be capable of carrying out dimerization of the two clusters, yielding a diamagnetic product with an $Fe(I)_2S_2$ core. Herein, the possible initial dimer structure is generated and displayed in Figure 6A,B. To drive the dimerization process, the RC was defined as the formation of two new Fe−S bonds while dissociating from the Met side chains as $0.612\ d(Fe_a{-}S_b) + 0.493\ d(Fe_b{-}S_a) - 0.204d(Fe_b{-}S_{M224}) - 0.583d(Fe_a{-}S_{M291})$, where the subscripts "*a*" and "*b*" refer to the complexes initially coordinated to M291 and M224, respectively. The coefficients were determined by harmonic linear discriminant analysis, an approach for determining the optimal collective variable based on the fluctuations of the reactant and product structures.[54] This RC has a large range due to the large distance changes, and over 80 umbrella sampling windows were required.

According to the energy profile in Figure S16, the dimerization process in HydE is kinetically and thermodynamically favorable with $(\Delta G^{\ddagger}, \Delta G) \sim (15.1, -3)$ kcal/mol. The spin population of the two Fe atoms stays around −1.2 and +1.1, respectively, across the entire RC, showing that there is no qualitative change in the unpaired electron density, and the final product contains two antiferromagnetically coupled Fe(I) atoms, which is consistent with the super-reduced state of the $[2Fe]_H$ cluster in [FeFe]-hydrogenase.[55] Therefore, we can assert that our results are consistent with the EPR experimental results in which no signal would indicate a paramagnetic dimer product. Such diamagnetic species could be identified by infrared spectroscopy using the CO/CN ligands as vibrational probes.[56−60] The key structures and the key distances during the reactions are drawn in Figures 6 and S16. The analysis shows large fluctuations in the $Fe_a{-}S_b$ bond distance between bonding and nonbonding regimes, indicating that the $[Fe(I)(CO)_2(CN)(SH)]$ species are highly labile. Both clusters are fully dissociated from their host methionine residues before formation of the $Fe_a{-}S_b$ and $Fe_b{-}S_a$ bonds in the dimer.

The dimerization product is located in the cavity between M291 and M224 (Figure 6C). The small cavity is relatively hydrophobic, preventing water molecules from entering and binding to the unsaturated Fe clusters. The isobutyl side chain of L157, the isopropyl side chain of V105, and the dimethyl sulfide side chain of M291 contribute to the creation of this hydrophobic cavity, and the diatomic ligands on the Fe(I) cluster occupy much of the remaining space. As a result, the few water molecules near the two Fe(I) clusters are mostly concentrated around the remaining 5′-dAdo. Moreover, our calculations showed that if the penta-coordinate Fe(I) cluster was exposed to solvent, water forms a strong coordination bond that is difficult to release (Figure S17). Outside the hydrophobic cavity, several polar residues, namely, R54, T134, R155, and T269, contact the CN ligands via hydrogen bonds or electrostatic interactions. The secondary coordination sphere around the CN ligands plays a key role in facilitating H_2 generation in the [FeFe]-hydrogenase.[61] This computational evidence supports the dimerization of Fe(I) clusters in HydE before delivery to HydF.

4. CONCLUSIONS

In this article, we have proposed a complete mechanism for the catalytic cycle of HydE, in which two equivalents of an $[Fe(II)(Cys)(CO)_2(CN)]$ substrate are converted to a diamagnetic $[Fe(I)_2(SH)_2(CO)_4(CN)_2]$ complex. The reaction is initialized with typical SAM decomposition but immediately followed by an unconventional C−S radical addition to form a "10 s intermediate" containing $[Fe(I)(CO)_2(CN)(SAC)]$. The decomposition of the "10 s intermediate" likely occurs through a radical relay pathway involving homolytic cleavage of the S−Cβ bond on the SAC ligand rather than a closed-shell proton-transfer pathway, as the former has a much lower free energy barrier and preserves consistency with experiments. We further found that the decomposition involves the release of pyruvate, matching the experimental observation.

An overall theme can be seen regarding the mechanism of HydE in how it cleaves the S−Cβ and S−C5 bonds of the "10 s intermediate" and "10 min intermediate" respectively, which are the most difficult elementary steps in the entire reaction; in particular, the redox-active Fe(I) center of the substrate enables radical chemistry to be performed in the first coordination sphere. At the start of the catalytic cycle, the attack of 5′-dAdo$^{\bullet}$ on Syn-B reduces Fe(II) to Fe(I) and causes the Fe−S bond to dissociate, leading to the "10 s intermediate". The first step in the conversion of the "10 s intermediate" is an "inverse radical attack" that cleaves the S−Cβ bond instead of the S−C5 bond and oxidizes Fe(I) back to Fe(II); the radical is eventually transferred back to the Fe center, yielding Fe(I) again. This pathway is invoked again when transferring 5′-dAdo substituted from SH to OH; by "inverse radical attack", the S−C5 bond is cleaved, oxidizing Fe(I) to Fe(II) and yielding 5′-dAdo$^{\bullet}$, which then attacks the hydroxyl ligand, yielding adenosine and completing the transfer.

We have also proposed an energetically feasible mechanism for the dimerization of two Fe(I) complexes catalyzed by HydE. With the help of two methionines, namely, M224 and M291, HydE is able to accommodate two single-Fe clusters simultaneously, and the dimerization was shown to be thermodynamically and kinetically favorable. We have also discussed other advantages of dimerization in HydE, such as the relative hydrophobic environment and the favorable relative positioning and orientation of the two atoms within the protein. The species $[Fe_2(\mu\text{-}SH)_2(CN)_2(CO)_4]^{2-}$ is proposed to be the final product of HydE, and already contains several key elements of the final product of the HydG-HydE-HydF assembly line, that is, the H-cluster that forms the active site of [FeFe]-hydrogenase.

■ ASSOCIATED CONTENT

Supporting Information

The Supporting Information is available free of charge at https://pubs.acs.org/doi/10.1021/jacs.4c12668.

Details of all individual reaction steps including free energy profiles and 3D representations of structures within the protein environment; description of unconventional β-elimination pathway for cysteinyl Cβ−S cleavage; and comparison with radical pathway (PDF)

■ AUTHOR INFORMATION

Corresponding Authors

R. David Britt − *Department of Chemistry, University of California Davis, Davis, California 95616, United States;* orcid.org/0000-0003-0889-8436; Email: rdbritt@ucdavis.edu

Lee-Ping Wang − *Department of Chemistry, University of California Davis, Davis, California 95616, United States;*

https://doi.org/10.1021/jacs.4c12668
J. Am. Chem. Soc. 2025, 147, 4800−4809

orcid.org/0000-0003-3072-9946; Email: leeping@ucdavis.edu

Authors

Nanhao Chen − *Department of Chemistry, University of California Davis, Davis, California 95616, United States;* Present Address: Peking University, Beijing 100871, China

Guodong Rao − *Department of Chemistry, University of California Davis, Davis, California 95616, United States;* orcid.org/0000-0001-8043-3436

Lizhi Tao − *Department of Chemistry, University of California Davis, Davis, California 95616, United States;* Present Address: Southern University of Science and Technology, Shenzhen 518055, China.; orcid.org/0000-0001-9921-2297

Complete contact information is available at: https://pubs.acs.org/10.1021/jacs.4c12668

Notes

The authors declare no competing financial interest.

■ ACKNOWLEDGMENTS

R.D.B. acknowledges funding support from NIH R35GM126961. L.P.W. acknowledges funding support from ARO award number W911NF1710434. This paper is adapted from a chapter of N.C.'s Ph.D. dissertation.

■ REFERENCES

(1) Vignais, P. M.; Billoud, B. Occurrence, classification, and biological function of hydrogenases: an overview. *Chem. Rev.* **2007**, *107*, 4206−4272.

(2) Vincent, K. A.; Parkin, A.; Armstrong, F. A. Investigating and exploiting the electrocatalytic properties of hydrogenases. *Chem. Rev.* **2007**, *107*, 4366−4413.

(3) Lubitz, W.; Ogata, H.; Rudiger, O.; Reijerse, E. Hydrogenases. *Chem. Rev.* **2014**, *114*, 4081−4148.

(4) Zhou, P.; Navid, I. A.; Ma, Y.; Xiao, Y.; Wang, P.; Ye, Z.; Zhou, B.; Sun, K.; Mi, Z. Solar-to-hydrogen efficiency of more than 9% in photocatalytic water splitting. *Nature* **2023**, *613*, 66−70.

(5) Kuchenreuther, J. M.; Britt, R. D.; Swartz, J. R. New Insights into [FeFe] Hydrogenase Activation and Maturase Function. *PLoS One* **2012**, *7*, No. e45850.

(6) Kuchenreuther, J. M.; Myers, W. K.; Stich, T. A.; George, S. J.; NejatyJahromy, Y.; Swartz, J. R.; Britt, R. D. A radical intermediate in tyrosine scission to the CO and CN- ligands of FeFe hydrogenase. *Science* **2013**, *342*, 472−475.

(7) Kuchenreuther, J. M.; Guo, Y.; Wang, H.; Myers, W. K.; George, S. J.; Boyke, C. A.; Yoda, Y.; Alp, E. E.; Zhao, J.; Britt, R. D.; et al. Nuclear resonance vibrational spectroscopy and electron paramagnetic resonance spectroscopy of 57Fe-enriched [FeFe] hydrogenase indicate stepwise assembly of the H-cluster. *Biochemistry* **2013**, *52*, 818−826.

(8) Kuchenreuther, J. M.; Myers, W. K.; Suess, D. L.; Stich, T. A.; Pelmenschikov, V.; Shiigi, S. A.; Cramer, S. P.; Swartz, J. R.; Britt, R. D.; George, S. J. The HydG enzyme generates an Fe (CO) 2 (CN) synthon in assembly of the FeFe hydrogenase H-cluster. *Science* **2014**, *343*, 424−427.

(9) Myers, W. K.; Stich, T. A.; Suess, D. L.; Kuchenreuther, J. M.; Swartz, J. R.; Britt, R. D. The cyanide ligands of [FeFe] hydrogenase: Pulse EPR studies of 13C and 15N-labeled H-cluster. *J. Am. Chem. Soc.* **2014**, *136*, 12237−12240.

(10) Dinis, P.; Suess, D. L.; Fox, S. J.; Harmer, J. E.; Driesener, R. C.; De La Paz, L.; Swartz, J. R.; Essex, J. W.; Britt, R. D.; Roach, P. L. X-ray crystallographic and EPR spectroscopic analysis of HydG, a maturase in [FeFe]-hydrogenase H-cluster assembly. *Proc. Natl. Acad. Sci. U.S.A.* **2015**, *112*, 1362−1367.

(11) Suess, D. L.; Bürstel, I.; De La Paz, L.; Kuchenreuther, J. M.; Pham, C. C.; Cramer, S. P.; Swartz, J. R.; Britt, R. D. Cysteine as a ligand platform in the biosynthesis of the FeFe hydrogenase H cluster. *Proc. Natl. Acad. Sci. U.S.A.* **2015**, *112*, 11455−11460.

(12) Suess, D. L.; Kuchenreuther, J. M.; De La Paz, L.; Swartz, J. R.; Britt, R. D. Biosynthesis of the [FeFe] hydrogenase H cluster: A central role for the radical SAM enzyme HydG. *Inorg. Chem.* **2016**, *55*, 478−487.

(13) Suess, D. L.; Pham, C. C.; Bürstel, I.; Swartz, J. R.; Cramer, S. P.; Britt, R. D. The radical SAM enzyme HydG requires cysteine and a dangler iron for generating an organometallic precursor to the [FeFe]-hydrogenase H-cluster. *J. Am. Chem. Soc.* **2016**, *138*, 1146−1149.

(14) Peters, J. W.; Lanzilotta, W. N.; Lemon, B. J.; Seefeldt, L. C. X-ray crystal structure of the Fe-only hydrogenase (CpI) from Clostridium pasteurianum to 1.8 angstrom resolution. *Science* **1998**, *282*, 1853−1858.

(15) Nicolet, Y.; Piras, C.; Legrand, P.; Hatchikian, C. E.; Fontecilla-Camps, J. C. Desulfovibrio desulfuricans iron hydrogenase: the structure shows unusual coordination to an active site Fe binuclear center. *Structure* **1999**, *7*, 13−23.

(16) McGlynn, S. E.; Mulder, D. W.; Shepard, E. M.; Broderick, J. B.; Peters, J. W. Hydrogenase cluster biosynthesis: organometallic chemistry nature's way. *Dalton Trans.* **2009**, 4274−4285.

(17) Kuchenreuther, J. M.; Stapleton, J. A.; Swartz, J. R. Tyrosine, cysteine, and S-adenosyl methionine stimulate in vitro [FeFe] hydrogenase activation. *PLoS One* **2009**, *4*, No. e7565.

(18) Mulder, D. W.; Boyd, E. S.; Sarma, R.; Lange, R. K.; Endrizzi, J. A.; Broderick, J. B.; Peters, J. W. Stepwise [FeFe]-hydrogenase H-cluster assembly revealed in the structure of HydAΔEFG. *Nature* **2010**, *465*, 248−251.

(19) Mulder, D. W.; Shepard, E. M.; Meuser, J. E.; Joshi, N.; King, P. W.; Posewitz, M. C.; Broderick, J. B.; Peters, J. W. Insights into [FeFe]-hydrogenase structure, mechanism, and maturation. *Structure* **2011**, *19*, 1038−1052.

(20) Kuchenreuther, J. M.; George, S. J.; Grady-Smith, C. S.; Cramer, S. P.; Swartz, J. R. Cell-free H-cluster synthesis and [FeFe] hydrogenase activation: all five CO and CN- ligands derive from tyrosine. *PLoS One* **2011**, *6*, No. e20346.

(21) Frey, P. A.; Booker, S. J. Radical mechanisms of S-adenosylmethionine-dependent enzymes. *Adv. Protein Chem.* **2001**, *58*, 1−45.

(22) Frey, M. Hydrogenases: hydrogen-activating enzymes. *ChemBioChem* **2002**, *3*, 153−160.

(23) Frey, P. A.; Hegeman, A. D.; Ruzicka, F. J. The radical SAM superfamily. *Crit. Rev. Biochem. Mol. Biol.* **2008**, *43*, 63−88.

(24) Duffus, B. R.; Ghose, S.; Peters, J. W.; Broderick, J. B. Reversible H atom abstraction catalyzed by the radical S-adenosylmethionine enzyme HydG. *J. Am. Chem. Soc.* **2014**, *136*, 13086−13089.

(25) Chen, N.; Rao, G.; Britt, R. D.; Wang, L.-P. Quantum Chemical Study of a Radical Relay Mechanism for the HydG-Catalyzed Synthesis of a Fe(II)(CO)2(CN)cysteine Precursor to the H-Cluster of [FeFe] Hydrogenase. *Biochemistry* **2021**, *60*, 3016−3026.

(26) Rao, G.; Pattenaude, S. A.; Alwan, K.; Blackburn, N. J.; Britt, R. D.; Rauchfuss, T. B. The binuclear cluster of [FeFe] hydrogenase is formed with sulfur donated by cysteine of an [Fe(Cys)(CO)(2)(CN)] organometallic precursor. *Proc. Natl. Acad. Sci. U.S.A.* **2019**, *116*, 20850−20855.

(27) Omeiri, J.; Martin, L.; Usclat, A.; Cherrier, M. V.; Nicolet, Y. Maturation of the [FeFe]-Hydrogenase: Direct Transfer of the (κ 3-cysteinate)FeII(CN)(CO)2 Complex B from HydG to HydE. *Angew. Chem., Int. Ed.* **2023**, *62*, No. e202314819.

(28) Berggren, G.; Adamska, A.; Lambertz, C.; Simmons, T. R.; Esselborn, J.; Atta, M.; Gambarelli, S.; Mouesca, J.-M.; Reijerse, E.; Lubitz, W.; Happe, T.; Artero, V.; Fontecave, M. Biomimetic assembly and activation of [FeFe]-hydrogenases. *Nature* **2013**, *499*, 66−69.

(29) Rao, G.; Tao, L.; Britt, R. D. Serine is the molecular source of the NH(CH2)2 bridgehead moiety of the in vitro assembled [FeFe] hydrogenase H-cluster. *Chem. Sci.* **2020**, *11*, 1241−1247.

(30) Pagnier, A.; Balci, B.; Shepard, E. M.; Yang, H.; Warui, D. M.; Impano, S.; Booker, S. J.; Hoffman, B. M.; Broderick, W. E.; Broderick, J. B. [FeFe]-Hydrogenase: Defined Lysate-Free Maturation Reveals a Key Role for Lipoyl-H-Protein in DTMA Ligand Biosynthesis. *Angew. Chem., Int. Ed.* **2022**, *61*, No. e202203413.
(31) Balci, B.; O'Neill, R. D.; Shepard, E. M.; Pagnier, A.; Marlott, A.; Mock, M. T.; Broderick, W. E.; Broderick, J. B. Semisynthetic maturation of [FeFe]-hydrogenase using [Fe 2 (μ-SH) 2 (CN) 2 (CO) 4] 2-: key roles for HydF and GTP. *Chem. Commun.* **2023**, *59*, 8929−8932.
(32) Esselborn, J.; Lambertz, C.; Adamska-Venkatesh, A.; Simmons, T.; Berggren, G.; Noth, J.; Siebel, J.; Hemschemeier, A.; Artero, V.; Reijerse, E.; Fontecave, M.; Lubitz, W.; Happe, T. Spontaneous activation of [FeFe]-hydrogenases by an inorganic [2Fe] active site mimic. *Nat. Chem. Biol.* **2013**, *9*, 607−609.
(33) Tao, L.; Pattenaude, S. A.; Joshi, S.; Begley, T. P.; Rauchfuss, T. B.; Britt, R. D. Radical SAM Enzyme HydE Generates Adenosylated Fe(I) Intermediates En Route to the [FeFe]-Hydrogenase Catalytic H-Cluster. *J. Am. Chem. Soc.* **2020**, *142*, 10841−10848.
(34) Rohac, R.; Martin, L.; Liu, L.; Basu, D.; Tao, L.; Britt, R. D.; Rauchfuss, T. B.; Nicolet, Y. Crystal Structure of the [FeFe]-Hydrogenase Maturase HydE Bound to Complex-B. *J. Am. Chem. Soc.* **2021**, *143*, 8499−8508.
(35) Britt, R. D.; Tao, L.; Rao, G.; Chen, N.; Wang, L.-P. Proposed Mechanism for the Biosynthesis of the [FeFe] Hydrogenase H-Cluster: Central Roles for the Radical SAM Enzymes HydG and HydE. *ACS Bio Med Chem Au* **2022**, *2*, 11−21.
(36) Britt, R. D.; Rauchfuss, T. B.; Rao, G. The H-cluster of [FeFe] Hydrogenases: Its Enzymatic Synthesis and Parallel Inorganic Semi-synthesis. *Acc. Chem. Res.* **2024**, *57*, 1941−1950.
(37) Zhang, Y.; Tao, L.; Woods, T. J.; Britt, R. D.; Rauchfuss, T. B. Organometallic Fe2(μ -SH)2(CO)4(CN)2 Cluster Allows the Biosynthesis of the [FeFe]-Hydrogenase with Only the HydF Maturase. *J. Am. Chem. Soc.* **2022**, *144*, 1534−1538.
(38) Wang, L.-P.; McKiernan, K. A.; Gomes, J.; Beauchamp, K. A.; Head-Gordon, T.; Rice, J. E.; Swope, W. C.; Martínez, T. J.; Pande, V. S. Building a more predictive protein force field: a systematic and reproducible route to AMBER-FB15. *J. Phys. Chem. B* **2017**, *121*, 4023−4039.
(39) Wang, L.-P.; Martinez, T. J.; Pande, V. S. Building Force Fields: An Automatic, Systematic, and Reproducible Approach. *J. Phys. Chem. Lett.* **2014**, *5*, 1885−1891.
(40) Wang, J.; Wolf, R. M.; Caldwell, J. W.; Kollman, P. A.; Case, D. A. Development and testing of a general amber force field. *J. Comput. Chem.* **2004**, *25*, 1157−1174.
(41) Chang, C. H.; Kim, K. Density functional theory calculation of bonding and charge parameters for molecular dynamics studies on [FeFe] hydrogenases. *J. Chem. Theory Comput.* **2009**, *5*, 1137−1145.
(42) Li, Z.; Song, L. F.; Li, P.; Merz, K. M., Jr. Systematic parametrization of divalent metal ions for the OPC3, OPC, TIP3P-FB, and TIP4P-FB water models. *J. Chem. Theory Comput.* **2020**, *16*, 4429−4442.
(43) Case, D. A.; Cheatham III, T. E.; Darden, T.; Gohlke, H.; Luo, R.; Merz, K. M., Jr.; Onufriev, A.; Simmerling, C.; Wang, B.; Woods, R. J. The Amber biomolecular simulation programs. *J. Comput. Chem.* **2005**, *26*, 1668−1688.
(44) Shao, Y.; et al. Advances in molecular quantum chemistry contained in the Q-Chem 4 program package. *Mol. Phys.* **2015**, *113*, 184−215.
(45) Zhou, Y.; Wang, S.; Li, Y.; Zhang, Y. *Methods in Enzymology*; Elsevier, 2016; Vol. *577*, pp 105−118.
(46) Zhao, C.; Li, Y.; Wang, C.; Chen, H. Mechanistic dichotomy in the activation of SAM by radical SAM enzymes: QM/MM modeling deciphers the determinant. *ACS Catal.* **2020**, *10*, 13245−13250.
(47) Zhang, Y. Pseudobond ab initio QM/MM approach and its applications to enzyme reactions. *Theor. Chem. Acc.* **2006**, *116*, 43−50.
(48) Roux, B. The calculation of the potential of mean force using computer simulations. *Comput. Phys. Commun.* **1995**, *91*, 275−282.
(49) Grossfield, A. *An Implementation of WHAM: The Weighted Histogram Analysis Method*; Grossfield Lab, version 2.0.9, 2014. http://membrane.urmc.rochester.edu/content/wham/.
(50) Alexandrova, A. N.; Jorgensen, W. L. On the Mechanism and Rate of Spontaneous Decomposition of Amino Acids. *J. Phys. Chem. B* **2011**, *115*, 13624−13632.
(51) Zhou, S.; Wei, W.-J.; Liao, R.-Z. QM/MM Study of the Mechanism of the Noncanonical S-Cγ Bond Scission in S-Adenosylmethionine Catalyzed by the CmnDph2 Radical Enzyme. *Top. Catal.* **2022**, *65*, 517−527.
(52) Grady, J. K.; Chasteen, N.; Harris, D. C. Radicals from "Good's" buffers. *Anal. Biochem.* **1988**, *173*, 111−115.
(53) Chovancova, E.; Pavelka, A.; Benes, P.; Strnad, O.; Brezovsky, J.; Kozlikova, B.; Gora, A.; Sustr, V.; Klvana, M.; Medek, P.; Biedermannova, L.; Sochor, J.; Damborsky, J. CAVER 3.0: A Tool for the Analysis of Transport Pathways in Dynamic Protein Structures. *PLoS Comput. Biol.* **2012**, *8*, No. e1002708.
(54) Mendels, D.; Piccini, G.; Parrinello, M. Collective Variables from Local Fluctuations. *J. Phys. Chem. Lett.* **2018**, *9*, 2776−2781.
(55) Lubitz, W.; Reijerse, E.; van Gastel, M. [NiFe] and [FeFe] hydrogenases studied by advanced magnetic resonance techniques. *Chem. Rev.* **2007**, *107*, 4331−4365.
(56) Mulder, D. W.; Ratzloff, M. W.; Bruschi, M.; Greco, C.; Koonce, E.; Peters, J. W.; King, P. W. Investigations on the role of proton-coupled electron transfer in hydrogen activation by [FeFe]-hydrogenase. *J. Am. Chem. Soc.* **2014**, *136*, 15394−15402.
(57) Mebs, S.; Senger, M.; Duan, J.; Wittkamp, F.; Apfel, U.-P.; Happe, T.; Winkler, M.; Stripp, S. T.; Haumann, M. Bridging hydride at reduced H-cluster species in [FeFe]-hydrogenases revealed by infrared spectroscopy, isotope editing, and quantum chemistry. *J. Am. Chem. Soc.* **2017**, *139*, 12157−12160.
(58) Stripp, S. T.; Mebs, S.; Haumann, M. Temperature dependence of structural dynamics at the catalytic cofactor of [FeFe]-hydrogenase. *Inorg. Chem.* **2020**, *59*, 16474−16488.
(59) Mirmohades, M.; Adamska-Venkatesh, A.; Sommer, C.; Reijerse, E.; Lomoth, R.; Lubitz, W.; Hammarstrom, L. Following [FeFe] hydrogenase active site intermediates by time-resolved mid-IR spectroscopy. *J. Phys. Chem. Lett.* **2016**, *7*, 3290−3293.
(60) Sanchez, M. L.; Sommer, C.; Reijerse, E.; Birrell, J. A.; Lubitz, W.; Dyer, R. B. Investigating the kinetic competency of Cr HydA1 [FeFe] hydrogenase intermediate states via time-resolved infrared spectroscopy. *J. Am. Chem. Soc.* **2019**, *141*, 16064−16070.
(61) Lampret, O.; Adamska-Venkatesh, A.; Konegger, H.; Wittkamp, F.; Apfel, U.-P.; Reijerse, E. J.; Lubitz, W.; Rüdiger, O.; Happe, T.; Winkler, M. Interplay between CN− Ligands and the Secondary Coordination Sphere of the H-Cluster in [FeFe]-Hydrogenases. *J. Am. Chem. Soc.* **2017**, *139*, 18222−18230.

https://doi.org/10.1021/jacs.4c12668
J. Am. Chem. Soc. 2025, 147, 4800−4809